Korean J. Chem. Eng., 34(1), 189-198 (2017)
DOI: 10.1007/s11814-016-0213-4

pISSN: 0256-1115
eISSN: 1975-7220

Magnetic field effect on the onset of Soret-driven convection of a nanofluid confined within a Hele-Shaw cell

Min Chan Kim†

Department of Chemical Engineering, Jeju National University, Jeju 63243, Korea
(*Received 23 April 2016 • accepted 23 July 2016*)

Abstract−The effect of a magnetic field on the early stages of Soret-driven convection of a nanoparticle suspension with large negative separation ratio χ confined within a Hele-Shaw cell, heated from above, was analyzed. Taking the Lorentz force into account, new stability equations were formulated in a similar (τ, ζ)-domain as well as in a global (τ, z)-domain by introducing the Hele-Shaw Rayleigh number based on the Soret flux (Rs_H) and the Hele-Shaw Hartmann number (Ha_H). With and without the quasi-steadiness assumptions, the resulting stability equations were solved analytically by expanding the disturbances as a series of orthogonal functions, and also the numerical shooting method was used. The critical time of the onset of convection and the corresponding wave number were obtained as a function of Rs_H and Ha_H. It was found that the magnetic field plays a critical role in the onset of convective instability. The onset time increases with increasing Ha_H and decreasing Rs_H. The linear stability limits are independent of the solution methods, if the trial functions for the disturbance quantities are properly chosen. Based on the results of the linear stability analysis, a non-linear analysis was conducted using direct numerical simulations. The non-linear analysis revealed that the convective motion can be apparent far after the linear stability limit.

Keywords: Soret-driven Convection, Nanoparticle Suspension, Magnetic Field Effect, Hele-shaw Cell, Linear Stability Analysis, Non-linear Analysis

INTRODUCTION

Nanofluids have attracted a great deal of interest for their greatly enhanced thermal properties. Nanofluids denote colloidal suspension of metallic of non-metallic solid particles (of dimension 1-100 nm) into the base fluids. Experiments have shown significant increases in thermal conductivity compared to traditional liquids without nanoparticles or to solid/liquid suspensions with larger particles and to the predictions of well-established theories. Taylor et al. [1] gave a good review for the applications of the nanofluids. Another important phenomenon in the nanofluids is the thermal diffusion due to the Soret effect. Particles move to the hotter region or to the colder one according to the sign of the Soret diffusion coefficient.

The onset of convective instability in a fluid driven by nanoparticle movement due to Soret effect was studied by Ryskin and Pleiner [2]. They examined thermally driven convection under the assumption of the linear and time-independent temperature and concentration profiles. Through their analysis, it can be concluded that the nanoparticle suspension system can be unstable if $Ra(\chi/Le)\geq 720$. This means that for the negative separation ratio case the system can be unstable even if $Ra<0$. However, for $Ra(\chi/Le)>>720$, experimental studies on the onset of Soret-driven transient convection were conducted by Cerbino et al. [3-5], Mazzoni et al. [6], Winkel et al. [7] and Messlinger et al. [8]. In this case the convective motion can be set in under the transient concentration field. Kim et al. [9], Kim and Choi [10], and Kim [11,12] investigated the transient analysis of the onset of Soret-driven convection in nanoparticle suspensions heated from above based on the linear stability theory and the energy method. They obtained that for small time the critical wavelength becomes smaller with increasing Rayleigh number based on Soret flux, while for large time a long wave mode is the most unstable mode. Recently, Messlinger et al. [13] analyzed the onset of Soret-driven convection in a bulk fluid, in a porous medium, and in a Hele-Shaw cell by extending Howard's [14] boundary layer instability concept. A comparison between Soret convection in a porous medium and in a narrow cell was given by Schöpf [15], who suggested that the assumption of zero permeability is usually a very good approximation for a porous medium. Although Messlinger et al's [13] and Schöpf's [15] analyses are simple and give a good scaling relation of the onset of Soret-driven convection, they do not consider the temporal evolution of disturbance quantities, and oversimplify the base concentration profile. Furthermore, they employ the steady state stability condition as a stability criterion for the transient problem. Therefore, their analysis lacks physical concepts of the onset of convective motion. Kim [16] conducted systematic analysis on the onset of Soret-driven convection in a horizontal porous medium or in a vertical Hele-Shaw cell.

It has been known that the magnetic field plays a critical role in the onset of Bénard-Rayleigh convection [17]. Also, similar researches have been conducted in a porous medium [18]. Heidary et al. [19] analyzed the magnetic field effect on nano-fluid forced convection in a channel numerically. However, the effect of a magnetic field on the onset of Soret-driven convection has never been analyzed.

†To whom correspondence should be addressed.
E-mail: mckim@jejunu.ac.kr

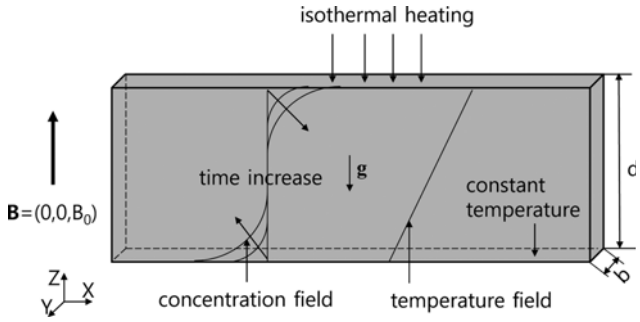

Fig. 1. Schematic diagram of system considered here. Magnetic field is uniform in the vertical Z-direction.

In the present study, we investigated the effect of a uniform vertical magnetic field on the onset of Soret-driven convection in the nanoparticles suspension confined within the vertical Hele-Shaw cell heated from above by employing linear stability analysis and nonlinear direct numerical simulations.

SYSTEMS AND GOVERNING EQUATIONS

The system considered here is an electrically conducting fluid contained in a Hele-Shaw cell under a uniform magnetic field. A non-magnetic nanoparticles suspended in a fluid and the initial particle concentration is C_i. For time t≥0, the horizontal layer of depth d is heated from above with a constant temperature T_u and its lower boundary is kept at the initial temperature T_i. The schematic diagram of the basic system of pure diffusion is shown in Fig. 1. For a sufficiently small thickness, b<<d, the flow can be approximated as a two-dimensional Stokes flow in the X-Z-plane, commonly referred to as Hele-Shaw flow by Schöpf [15], which is widely used to simulate flow in a porous medium. Under the Hele-Shaw approximation, the governing equations to describe the Boussinesq flow in a Hele-Shaw cell are [15]:

$$\nabla\cdot\mathbf{U}=0, \tag{1}$$

$$\frac{\mu}{\mathrm{K}}\mathbf{U}=-\nabla\mathrm{P}+\rho_i\mathbf{g}\{-\beta_T(\mathrm{T}-\mathrm{T}_i)+\beta_c(\mathrm{C}-\mathrm{C}_i)\}+\mathbf{J}\times\mathbf{B}, \tag{2}$$

$$\left\{\frac{\partial}{\partial \mathrm{t}}+\mathbf{U}\cdot\nabla\right\}\mathrm{T}=\alpha\nabla^2\mathrm{T}, \tag{3}$$

$$\left\{\frac{\partial}{\partial \mathrm{t}}+\mathbf{U}\cdot\nabla\right\}\mathrm{C}=-\nabla^2\cdot\mathbf{j}, \tag{4}$$

$$\mathbf{j}=\mathbf{j}_D+\mathbf{j}_S=-(\mathrm{D}_C\nabla\mathrm{C}+\mathrm{D}_T\nabla\mathrm{T}), \tag{5}$$

with the following initial and boundary conditions:

$$\mathbf{U}=0,\ \mathrm{T}=\mathrm{T}_i,\ \mathrm{C}=\mathrm{C}_i \text{ at } \mathrm{t}=0, \tag{6a}$$

$$\mathbf{U}=0,\ \mathrm{T}=\mathrm{T}_i,\ \mathrm{D}_C\frac{\partial \mathrm{C}}{\partial \mathrm{Z}}+\mathrm{D}_T\frac{\partial \mathrm{T}}{\partial \mathrm{Z}}=0 \text{ at } \mathrm{Z}=0, \tag{6b}$$

$$\mathbf{U}=0,\ \mathrm{T}=\mathrm{T}_u,\ \mathrm{D}_C\frac{\partial \mathrm{C}}{\partial \mathrm{Z}}+\mathrm{D}_T\frac{\partial \mathrm{T}}{\partial \mathrm{Z}}=0 \text{ at } \mathrm{Z}=\mathrm{d}, \tag{6c}$$

where **U** is the velocity, K (=b^2/12) has the meaning of the permeability of a porous medium, μ is the viscosity, P is the pressure, α is the thermal diffusivity, **J** is the electric current density and **B** is the magnetic field. Note that the Lorentz force term **J**×**B** is included in the momentum Eq. (2). Here, we consider only the case **B**=$B_0\mathbf{e}_z$, that is, **B** directed in the upward *z*-direction, with the fluid occupying the layer 0≤Z≤d. As discussed by Galoi and Straughan [20] and Harfash [18], under the assumption of $D_C/\eta\to 0$ and (∇×**U**)·$\mathbf{e}_z$=0, here η is the magnetic diffusivity, **J**=σ(**U**×**B**), and therefore, the Lorentz force term in the momentum equation can be expressed as

$$\mathbf{J}\times\mathbf{B}=\sigma(\mathbf{U}\times\mathrm{B}_0\mathbf{e}_z)\times\mathrm{B}_0\mathbf{e}_z, \tag{7}$$

where σ is the electrical conductivity. In the Hele-Shaw approximation, **U**=[U (X, Z), 0 (=V), W (X, Z)] is employed and therefore, (∇×**U**)·$\mathbf{e}_z$=(∂V/∂X−∂U/∂Y)=0 is naturally satisfied.

For the present stability analysis, we define d, D_C/d, $D_C\mu$/K, d^2/D_C, j_Sd/D_C and $\Delta T=(T_i-T_u)$ as the length, velocity, pressure, time, concentration and temperature scaling factors, respectively. Here j_S=Δ_TDT/d is the mass flux due to the Soret effect. Then, the above governing Eqs. (1)-(7) can be rewritten in dimensionless forms as

$$\nabla\cdot\mathbf{u}=0, \tag{8}$$

$$\mathbf{u}=-\nabla\mathrm{p}-\left\{\mathrm{Rs}_H\mathrm{c}+\frac{\mathrm{Ra}_H}{\mathrm{Le}}\theta\right\}\mathbf{e}_z+\mathrm{Ha}_H^2(\mathbf{u}\times\mathbf{e}_z)\times\mathbf{e}_z, \tag{9}$$

$$\left\{\frac{\partial}{\partial\tau}+\mathbf{u}\cdot\nabla\right\}\theta=\frac{1}{\mathrm{Le}}\nabla^2\theta, \tag{10}$$

$$\left\{\frac{\partial}{\partial\tau}+\mathbf{u}\cdot\nabla\right\}\mathrm{c}=\nabla^2(\mathrm{c}-\theta), \tag{11}$$

under the following initial and boundary conditions:

$$\mathbf{u}=0,\ \theta=0,\ \mathrm{c}=0 \text{ at } \tau=0, \tag{12a}$$

$$\mathbf{u}=0,\ \theta=0,\ \frac{\partial}{\partial \mathrm{z}}(\mathrm{c}-\theta)=0 \text{ at } \mathrm{z}=0, \tag{12b}$$

$$\mathbf{u}=0,\ \theta=1,\ \frac{\partial}{\partial \mathrm{z}}(\mathrm{c}-\theta)=0 \text{ at } \mathrm{z}=1, \tag{12c}$$

Important parameters to describe the present system are the Lewis number, the Ryleigh number, the Hele-Shaw Rayleigh number, the separation ration, the Hele-Shaw Rayleigh number based on the Soret flux, j_S, and the Hele-Shaw Hartmann number defined as

$$\mathrm{Le}=\frac{\mathrm{D}_C}{\alpha},\ \mathrm{Ra}=\frac{\mathrm{g}\beta\Delta\mathrm{T}\mathrm{d}^3}{\alpha\nu},\ \mathrm{Ra}_H=\frac{\mathrm{g}\beta\Delta\mathrm{T}\mathrm{K}\mathrm{d}}{\alpha\nu},\ \chi=\frac{\beta_C\mathrm{D}_T}{\beta_T\mathrm{D}_C},$$
$$\mathrm{Rs}_H=\mathrm{Ra}_H\frac{\chi}{\mathrm{Le}},\ \text{and } \mathrm{Ha}_H=\mathrm{B}_0\left(\frac{\sigma\mathrm{K}}{\mu}\right)^{1/2}.$$

For the limiting case of Le→0, as discussed by Ryskin and Pleiner [2], Messlinger et al. [13], Kim et al. [9], Kim and Choi [10], and Kim [11,12], by considering the heat conduction and diffusion time scale, it can be assumed that there is always a fully developed stationary temperature profile for the extreme case of very small Le, i.e., temperature field can be assumed as

$$\theta=\mathrm{z}. \tag{13}$$

In this case, $\partial\theta/\partial$z=1 is hold and therefore (∂c/∂z)=1 is applied to both impermeable boundaries where **j**·$\mathbf{e}_z$=0. Therefore, the dimensionless governing equations are reduced as

$$\nabla\cdot\mathbf{u}=0, \tag{8}$$

$$\mathbf{u} = -\nabla\tilde{p} - \mathrm{Rs}_H c\mathbf{e}_z + \mathrm{Ha}_H^2(\mathbf{u}\times\mathbf{e}_z)\times\mathbf{e}_z, \tag{14}$$

$$\left\{\frac{\partial}{\partial\tau} + \mathbf{u}\cdot\nabla\right\}c = \nabla^2 c, \tag{15}$$

where $\nabla\tilde{p}=\nabla p+(\mathrm{zRa/Le})\mathbf{e}_z$. The initial and boundary conditions (12) can be rewritten as

$$\mathbf{u} = c = 0, \text{ at } \tau = 0, \tag{16a}$$

$$\mathbf{u} = 0, \frac{\partial c}{\partial z} = 1 \text{ at } z = 0 \text{ and } z = 1. \tag{16b}$$

For transient concentration field, the basic conduction state is represented in dimensionless form by

$$\frac{\partial c_0}{\partial\tau} = \frac{\partial^2 c_0}{\partial z^2}, \tag{17}$$

under the following initial and boundary conditions,

$$c_0(0, z) = 0 \text{ and } \frac{\partial c_0}{\partial z}(\tau, 0) = \frac{\partial c_o}{\partial z}(\tau, 1) = 1, \tag{18}$$

where c_0 is the dimensionless basic concentration. The boundary conditions have been obtained by the impermeable conditions for concentration at both boundaries, that is, $\mathbf{j}\cdot\mathbf{e}_z=0$ at Z=0 and d. The above equations can be solved by using the separation of variables and also the Laplace transform:

$$c_0(\tau, z) = z - \frac{1}{2} - \sum_{n=1}^{\infty}\frac{2((-1)^n-1)}{(n\pi)^2}\cos(n\pi z)\exp(-n^2\pi^2\tau), \tag{19a}$$

$$\begin{aligned} c_0(\tau, \zeta) = \sqrt{4\tau}\sum_{n=0}^{\infty}\Bigg\{ & -\mathrm{ierfc}\left(\frac{n}{\sqrt{\tau}} + \frac{\zeta}{2}\right) - \mathrm{ierfc}\left(\frac{n+1}{\sqrt{\tau}} - \frac{\zeta}{2}\right) \\ & + \mathrm{ierfc}\left(\frac{n+1/2}{\sqrt{\tau}} - \frac{\zeta}{2}\right) + \mathrm{ierfc}\left(\frac{n+1/2}{\sqrt{\tau}} + \frac{\zeta}{2}\right)\Bigg\}, \end{aligned} \tag{19b}$$

where $\zeta=z/\sqrt{\tau}$. These solutions satisfy the mass conservation law of $\frac{\partial}{\partial\tau}\left(\int_0^1 c_0 dz\right)=0$. The solution of c_0 in the (τ, ζ)-coordinates converges more rapidly than that in the (τ, z)-ones, especially for the case of small τ. For the deep-pool system of small τ ($\tau\le10^{-2}$) and ierfc(∞)=0, the basic concentration field is approximated by

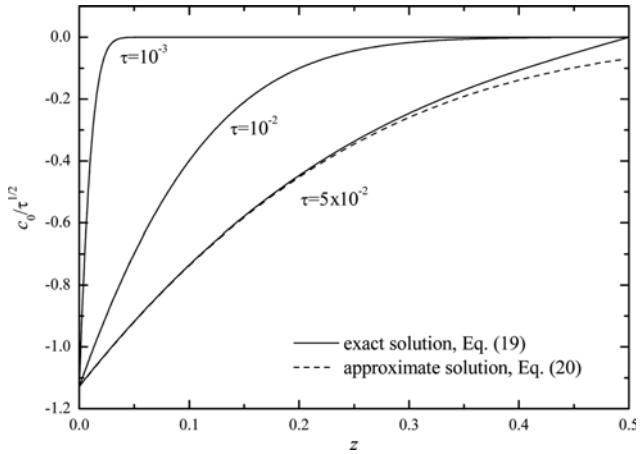

Fig. 2. Comparison of Eq. (20) with Eq. (19). For the difference between two equations becomes negligible.

$$c_0 = \sqrt{4\tau}\begin{cases} -\mathrm{ierfc}\left(\dfrac{z}{2\sqrt{\tau}}\right) & \text{for } z \le 1/2, \\ \mathrm{ierfc}\left(\dfrac{1-z}{2\sqrt{\tau}}\right) & \text{for } z \ge 1/2. \end{cases} \tag{20}$$

Here $-c_0(\tau, 0)=c_0(\tau, 1)=\sqrt{4\tau/\pi}$. The agreement with the exact solution is very good, as shown in Fig. 2. Eq. (19b) converges more rapidly than Eq. (19a) for a small time region. The evolution of the basic profiles of temperature with time is also shown in Fig. 2. The length $\delta(\tau)$, within which c_0 is non-zero, is the so-called 'penetration depth' of the diffusive boundary layer. The Leveque-type soution (20) is in good agreement with the exact solution (19) in the region of $\tau<0.01$.

LINEAR STABILITY ANALYSIS

1. Stability Equations

Under linear theory the disturbances caused by the onset of buoyancy-driven convection are formulated, in terms of the dimensionless disturbance concentration component c_1, and the dimensionless disturbance vertical velocity component by decomposing Eqs. (14)-(15):

$$\left\{(1+\mathrm{Ha}_H^2)\frac{\partial^2}{\partial z^2} - k^2\right\}w_1 = -\mathrm{Rs}_H k^2 c_1, \tag{21}$$

$$\frac{\partial c_1}{\partial\tau} + w_1\frac{\partial c_0}{\partial z} = \left(\frac{\partial^2}{\partial z^2} - k^2\right)c_1, \tag{22}$$

under the following boundary conditions:

$$w_1 = \frac{\partial c_1}{\partial z} = 0 \text{ at } z = 0 \text{ and } z = 1. \tag{23}$$

Here, the disturbances are decomposed into eigenfunctions, which depend on time and the streamwise coordinate, and Fourier modes in the *x*-direction with the wavenumber k.

As discussed by Messlinger et al. [13], Kim et al. [9], Kim and Choi [10], and Kim [11,12], in the deep-pool case of $\delta(\propto\sqrt{\tau})\ll1$, the concentration field near the lower and upper boundaries can be separable. Furthermore, by setting $z'=1-z$, the governing equations for the disturbance quantities near the upper boundary are identical to those near the lower one. In a semi-infinite domain where $\sqrt{\tau}\ll1$, the governing equations for the disturbance quantities near the lower boundary can be expressed as,

$$\left\{(1+\mathrm{Ha}_H^2)\frac{\partial^2}{\partial\zeta^2} - k^2\tau\right\}w_1 = -k^2\tau\mathrm{Rs}_H c_1, \tag{24}$$

$$\tau\frac{\partial c_1}{\partial\tau} - (L_\zeta - k^2\tau)c_1 = \tau w_1\mathrm{erfc}\left(\frac{\zeta}{2}\right). \tag{25}$$

The boundary conditions are transformed as

$$w_1 = \frac{\partial c_1}{\partial\zeta} = 0 \text{ at } \zeta = 0 \text{ and } \zeta\to\infty. \tag{26}$$

The diffusional operator in (τ, ζ)-domain L_ζ is

$$L_\zeta = \frac{\partial^2}{\partial\zeta^2} + \frac{\zeta}{2}\frac{\partial}{\partial\zeta}. \tag{27}$$

For the deep-pool case of small τ, the disturbances are localized mainly around the concentration front. However, in the (τ, z)-domain, the eigenfunctions of the diffusional operator $\partial^2/\partial z^2$ are not localized around the concentration fronts. Thus, in writing Eqs. (24)-(26), we have used a coordinate transformation into the similarity variable of the base state $\zeta=z/\sqrt{\tau}$ and the relation of $\partial/\partial\tau|_z=\partial/\partial\tau|_\zeta-1/(2\tau)\partial/\partial\zeta|_\tau$. By using $\zeta=(1-z)/\sqrt{\tau}$, exactly same equations can be derived near the upper boundary.

For the deep-pool case of $\delta(\propto\sqrt{\tau})<<1$, two sets of equations, Eqs. (21)-(23) and Eqs. (24)-(26), are mathematically equivalent except for non-analytic limit of $\tau=0$. Any semi-infinite domain solution produces the unrealistic limit of the infinite amplitude at $\tau=0$. However, the omission of $\tau=0$ does not cause any severe problem in the present analysis. This kind of coordinate transform has been widely used in similar problems [21-24].

2. Spectral Expansion

Here, we analyze the present system by solving Eqs. (24)-(26). To analyze systematically the growth of the disturbance, by using the property of generalized Fourier series, c_1 is expressed as [23]

$$c_1(\tau,\zeta)=\sum_{n=0}^{\infty}a_n(\tau)\kappa_n\phi_n(\zeta), \tag{28}$$

where κ_n is the normalization factor discussed later and ϕ_n are the orthonormal functions satisfying the following Sturm-Liouville boundary value problem:

$$L_\zeta\phi_n=-\lambda_n\phi_n, \tag{29}$$

under the following boundary conditions:

$$\frac{d\phi_n}{d\zeta}=0 \text{ at } \zeta=0 \text{ and } \zeta\to\infty. \tag{30}$$

The solutions of the above Sturm-Liouville boundary value problems, Eqs. (29) and (30), are

$$\phi_n=\kappa_n H_{2n}\left(\frac{\zeta}{2}\right)\exp\left(-\frac{\zeta^2}{4}\right) \text{ and } \lambda_n=-\frac{2n+1}{2}, \tag{31a}$$

$$\kappa_n=\left[\sqrt{2^{2n}\sqrt{\pi}\Gamma(2n+1)}\right]^{-1}, \tag{31b}$$

$$H_{2n}\left(\frac{\zeta}{2}\right)=(-1)^{2n}2^{2n}\exp\left(\frac{\zeta^2}{4}\right)\frac{d^{2n}}{d\zeta^{2n}}\left(\exp\left(-\frac{\zeta^2}{4}\right)\right), \tag{31c}$$

where $H_k(\xi)$ are the Hermite polynomials and the normalization factors κ_n is introduced to ensure the following orthonormal condition,

$$\kappa_m\kappa_n\int_0^\infty\phi_m\phi_n\exp\left(\frac{\zeta^2}{4}\right)d\zeta=\delta_{m,n}, \tag{32}$$

where $\exp(\zeta^2/4)$ is the weighting function of the Sturm-Liouville Eq. (29).

By combining Eqs. (24) and (28), we can get the following relation:

$$\left\{\frac{\partial^2}{\partial\zeta^2}-\frac{k^2\tau}{(1-Ha_H^2)}\right\}(w_1/Rs_H)=-\frac{k^2\tau}{(1+Ha_H^2)}\sum_{n=0}^{\infty}a_n(\tau)\kappa_n\phi_n(\zeta). \tag{33}$$

The solution of the Eq. (33) can be expressed as

$$\begin{aligned}(w_1/Rs_H)&=-k_H^{*2}\sum_{n=0}^{\infty}a_n(\tau)\kappa_n\left\{\frac{\partial^2}{\partial\zeta^2}-\frac{k^2\tau}{(1+Ha_H^2)}\right\}^{-1}\phi_n(\zeta)\\&=\sum_{n=0}^{\infty}a_n(\tau)\kappa_n\omega_n(\zeta),\end{aligned} \tag{34}$$

where ω_n's can be obtained by solving

$$(D^2-k_H^{*2})\omega_n(\zeta)=-k_H^{*2}\phi_n(\zeta), \tag{35a}$$

under the following boundary conditions,

$$\omega_n(0)=\omega_n(\infty)=0, \tag{35b}$$

where $D=\partial/\partial\zeta$ and $k_H^*=(k/\sqrt{1+Ha_H^2})\sqrt{\tau}$. The solution of Eq. (35) can be given as

$$\omega_n=-\frac{k_H^*}{2}\left[\begin{aligned}&\exp(k_H^*\zeta)\int_0^\zeta\exp\left(-k_H^*\xi-\frac{\xi^2}{4}\right)H_{2n}\left(\frac{\xi}{2}\right)d\xi\\&-\exp(k_H^*\zeta)\int_0^\zeta\exp\left(k_H^*\xi-\frac{\xi^2}{4}\right)H_{2n}\left(\frac{\xi}{2}\right)d\xi\\&-2\sinh\left((k_H^*\zeta)\int_0^\infty\exp\left(-k_H^*\xi-\frac{\xi^2}{4}\right)H_{2n}\left(\frac{\xi}{2}\right)d\xi\right)\end{aligned}\right], \tag{36}$$

After performing the integrations, Eq. (36) can be simplified recursively as

$$\omega_n=2^2k_H^{*2}(\omega_{n-1}-\phi_{n-1})+2^2k_H^{*2}[\exp(-k_H^*\zeta)H_{2n-2}(0)], \tag{37a}$$

with

$$\begin{aligned}\omega_0=\frac{k_H^*}{2}\sqrt{\pi}\exp(k_H^{*2})\Bigg[&\exp(k_H^*\zeta)\left\{\operatorname{erf}\left(\frac{\zeta}{2}+k_H^*\right)-1\right\}\\&-\exp(-k_H^*\zeta)\left\{\operatorname{erf}\left(\frac{\zeta}{2}-k_H^*\right)+2\operatorname{erf}(k_H^*)-1\right\}\Bigg].\end{aligned} \tag{37b}$$

Detailed procedure to obtain the solutions of (36)-(37) was already given by Kim and Choi [25].

Now, substituting for c_1 and w_1 from Eqs. (28) and (37) into Eq. (24), we obtain

$$\tau\sum_{n=0}^{\infty}\frac{da_n}{d\tau}\phi_n=-\sum_{n=0}^{\infty}(\lambda_n+k^{*2})a_n\phi_n+Rs_H\tau\operatorname{erfc}\left(\frac{\zeta}{2}\right)\sum_{n=0}^{\infty}a_n\omega_n. \tag{38}$$

By using the orthonormal property of $\phi_n(\zeta)$, multiplying Eq. (38) by $\exp(\zeta^2/4)\phi_m(\zeta)$ and integrating over the range of ζ, the following system of homogeneous linear equations for the constants a_n is obtained:

$$\begin{aligned}\tau\frac{da_m}{d\tau}=&-(\lambda_m+k^{*2})a_m\\&+Rs_H\tau\sum_{n=1}^{\infty}a_n\int_0^\infty\operatorname{erfc}\left(\frac{\zeta}{2}\right)\exp\left(\frac{\zeta^2}{4}\right)\phi_m(\zeta)\omega_n(\zeta)d\zeta.\end{aligned} \tag{39}$$

Now, Eq. (39) is written in the following matrix form:

$$\tau\frac{d\mathbf{a}}{d\tau}=\mathbf{E}\mathbf{a}, \tag{40}$$

where $\mathbf{a}=[a_0, a_1, \cdots]^T$, and the characteristic matrix $\mathbf{E}$ is

$$E_{mn}=-(\lambda_{m-1}+k^{*2})\delta_{m,n}+Rs_H\tau C_{mn}, \tag{41a}$$

$$C_{mn}=\int_0^{\infty}\mathrm{erfc}\left(\frac{\zeta}{2}\right)\exp\left(\frac{\zeta^2}{4}\right)\phi_{m-1}(\zeta)\omega_{n-1}(\zeta)\mathrm{d}\zeta. \tag{41b}$$

3. Solution Methods

3-1. Initial Growth Rate Analysis

Now, let us consider the initial growth rate of the disturbance. Regardless of Rs_H, for the limiting case of $\tau\to 0$, by neglecting higher order terms of τ, Eqs. (24) and (25) can be reduced as:

$$(1+Ha_H^2)\frac{\partial^2 w_1}{\partial\zeta^2}=0, \tag{42}$$

$$\tau\frac{\partial c_1}{\partial\tau}-L_\zeta c_1=0, \tag{43}$$

under the boundary conditions (26). The solution of Eq. (42) is

$$w_1\to 0 \text{ as } \tau\to 0. \tag{44}$$

This implies that the instabilities are not driven by the velocity disturbance. Also, from Eq. (29), we can get the following relation:

$$\tau\frac{\partial a_n}{\partial\tau}=-\lambda_n a_n \text{ as } \tau\to 0. \tag{45}$$

Among all the possible disturbance modes, the least damping mode is n=0 and corresponding eigenvalue is $\lambda_0=1/2$. This means that the following is the least stable disturbance:

$$c_1(\tau,\zeta)=a_0(\tau)\kappa_0\exp\left(-\frac{\zeta^2}{4}\right), \tag{46a}$$

and its initial growth rate is

$$\sigma^*\left(=\frac{1}{a_0}\frac{da_0}{d\tau}\right)=-\frac{\lambda_0}{\tau}=-\frac{1}{2\tau}. \tag{46b}$$

This initial disturbance also localized around the penetration depth, which is one of the most interesting findings of the present study: the most unstable mode of disturbance is determined in the deterministic functional form. Recently, for the limiting case of $Ha_H=0$, Noghrehabadi et al. [24] solved Eqs. (24) and (25) by introducing $c_1(\tau,\zeta)=\exp(-\zeta^2/4)$ at $\sqrt{\tau}Rs_H=0.1$. Thus, the present initial growth rate analysis provides the theoretical background for their numerical simulation. Another important finding is that the magnitude of initial disturbance is independent of Rs_H and Ha_H, since it is determined by $a_0(\tau)$ which depends on τ rather than Rs_H and Ha_H. This means that during the initial period, $a_0(\tau)=\{a_{0,i}\tau_i^{1/2}\}\tau^{-1/2}$ should be kept, regardless of Rs_H and Ha_H, where $a_{0,i}=a_0(\tau)$.

3-2. Generalized Stability Analysis (GSA)

Following the usual functional analysis [26], the norm of the disturbance $\|c_1\|$ is defined as

$$\|c_1\|=\left[\int_0^{\infty}c_1^2\exp\left(\frac{\zeta^2}{4}\right)\mathrm{d}\zeta\right]^{1/2}=\sqrt{\mathbf{a}^T\mathbf{a}}. \tag{47}$$

Here $\exp(\zeta^2/4)$ is inserted since it is the weighting function of the Sturm-Liouville equation (29). Based on this quantity, one can define the growth rate σ^* as

$$\sigma^*=\frac{1}{\|c_1\|}\frac{d\|c_1\|}{d\tau}=\frac{1}{2}\frac{1}{\mathbf{a}^T\mathbf{a}}\left(\frac{d\mathbf{a}^T}{d\tau}\mathbf{a}+\mathbf{a}^T\frac{d\mathbf{a}}{d\tau}\right). \tag{48}$$

Following Farrell and Ioannou's [27] GSA, the growth rate can be obtained as

$$\sigma^*\tau=\max\left\{\mathrm{eig}\left(\frac{\mathbf{E}+\mathbf{E}^T}{2}\right)\right\}. \tag{49}$$

For the limiting case of $\tau\to 0$, $\mathbf{E}_{mn}=\lambda_{m-1}\delta_{m,n}$ and its maximum eigenvalue is $\lambda_0=1/2$, i.e. $\sigma^*\tau=-1/2$, and corresponding eigenvector is $[1, 0, 0, \cdots]^T$, which is consistent with the results of the previous initial growth rate section (see Eq. (46)). Recently, Kim and Choi [28] discussed the effect of the choice of the norm on the growth rate and concluded that the choice of the norm does minor effect on the growth rate.

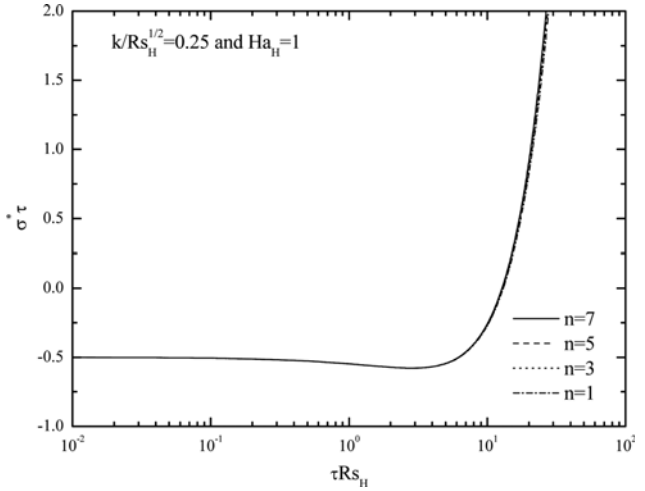

Fig. 3. Effect of the number of terms used in the eigen analysis in the domain.

For a specific case, the effect of the number of terms in the spectral analysis is summarized in Fig. 3. This figure shows that $\sigma^*\tau\to -1/2$ as $\tau\to 0$, regardless of the order of approximation. It also shows that for a small time region, seven-terms spectral approximation is quite enough to describe to the stability characteristics of the present system. As time increases, more terms are necessary to obtain more accurate growth rate.

3-3. Quasi-steady State Approximation (QSSA)

Here, under the quasi-steady state approximation in the (τ,ζ)-domain, it is assumed that the dimensionless amplitude functions of disturbances can be expressed as

$$[w_1(\tau,\zeta)/Rs_H, c_1(\tau,\zeta)]=[w_1^*(k^*,\zeta), c_1^*(\zeta)]\exp(\sigma^*\tau). \tag{50}$$

Under the QSSA, for the deep-pool region of $\sqrt{\tau}<<1$, i.e. in the semi-infinite domain, from the Eqs. (24), (25) and (50), the stability equations are approximated as

$$(D^2-k_H^{*2})w_1^*=-k_H^{*2}c_1^*, \tag{51}$$

$$\tau\sigma^* c_1^*=\left(D^2+\frac{\zeta}{2}D-k^{*2}\right)c_1^*+Rs_H\tau\mathrm{erfc}\left(\frac{\zeta}{2}\right)w_1^*, \tag{52}$$

under the following boundary conditions:

$$w_1^*=Dc_1^*=0 \text{ at } \zeta=0 \text{ and } \zeta\to\infty. \tag{53}$$

where $k^*=k\sqrt{\tau}$. Eqs. (51)-(53) can be solved by using the previous spectral expansion of c_1^* and w_1^*, and the growth rate in Eq. (49)

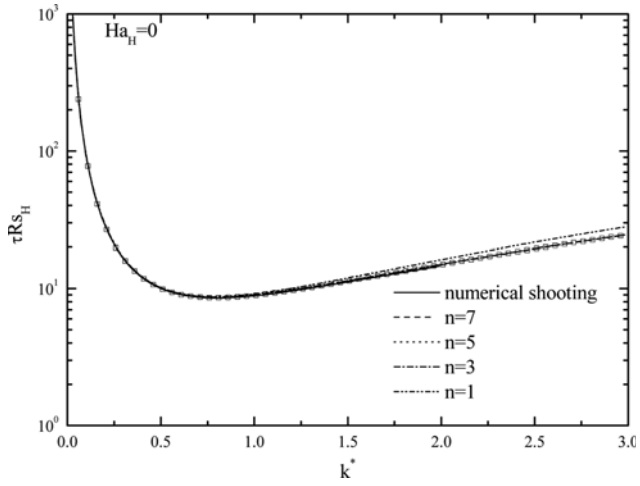

Fig. 4. The effect of the number of term n on the neutral stability curve based on the QSSA. □ Represents the neutral stability results based on the GSA with n=7.

can be approximated as

$$\sigma^{*}\tau=\max\{\mathrm{eig}(\mathbf{E})\}. \tag{54}$$

Also, the above stability Eqs. (51)-(53) are solved using the numerical shooting method [29]. By setting $\sigma^{*}=0$, the neutral stability curves for the case of $Ha_H=0$ are compared in Fig. 4. Fig. 4 suggests that for the deep-pool region, the analytic approximations and the numerical solution support with each other. Furthermore, because the present QSSA follows the GSA, Eq. (50) has a good theoretical background.

NONLINEAR PSEUDO-SPECTRAL ANALYSIS

1. Formulation

Although the above linear analyses give useful information on the growth of the instabilities, a more exact nonlinear solution can be obtained by solving Eqs. (1)-(3) directly. By expressing the velocity and concentration fields as $\mathbf{u}=(\partial\psi/\partial z, 0, -\partial\psi/\partial x)$, one can easily obtain the following dimensionless equation:

$$\frac{\partial^2\psi}{\partial x^2}+(1+\mathrm{Ha}_H^2)\frac{\partial^2\psi}{\partial z^2}=-\mathrm{Rs}_H\frac{\partial c}{\partial x}, \tag{55}$$

where ψ is a stream function. Also, by decomposing the concentration field as $c(\tau, x, z)=c_0(\tau, z)+c_1(\tau, x, z)$, Eqs. (8), (14) and (15) can be reduced as

$$\frac{\partial^2\psi}{\partial x^2}+(1+\mathrm{Ha}_H^2)\frac{\partial^2\psi}{\partial z^2}=-\mathrm{Rs}_H\frac{\partial c_1}{\partial x}, \tag{56}$$

$$\frac{\partial c_1}{\partial\tau}=\nabla^2 c_1-j, \tag{57}$$

$$j=\frac{\partial\psi}{\partial z}\frac{\partial c_1}{\partial x}-\frac{\partial\psi}{\partial x}\frac{\partial c_1}{\partial z}-\frac{\partial\psi}{\partial x}\frac{\partial c_0}{\partial z}, \tag{58}$$

where $c_0(\tau, z)$ is given in Eq. (19). The proper boundary conditions for Eqs. (56) and (57) are

$$\psi=\frac{dc_1}{dz}=0 \text{ at } z=0 \text{ and } z=1 \tag{59}$$

To take the advantage of the fast Fourier transform (FFT), by considering the governing equations and boundary conditions for ψ and c_1, the present problem defined in [0, 1] can be transformed into [−1/2, 1/2] by assuming that c_1 is an even function, and ψ and $\partial c_0/\partial c$ are odd functions satisfying the boundary conditions (59).

2. Fourier Spectral Method

Unlike the operator L_ζ defined in Eq. (14), the dominant diffusional operator in the (τ, z)-domain, $\partial^2/\partial z^2$ does not have the eigenfunctions that are localized around the thermal penetration depth. Therefore, the spectral method used in section 3.3 cannot be applied in the (τ, z)-domain. Here, Eqs. (60)-(64) are solved by the Fourier pseudo-spectral method which has been used in a similar problem [30]. Using the two-dimensional discrete Fourier transform (DFT), Eqs. (56) and (57) are transformed into the following ordinary differential equations:

$$[k_m^2+(1+\mathrm{Ha}_H^2)k_n^2]\hat{\psi}_{m,n}=\mathrm{Rs}_H ik_m\hat{c}_{m,n}, \tag{60}$$

$$\frac{d\hat{c}_{m,n}}{d\tau}=-(k_m^2+k_n^2)\hat{c}_{m,n}-\hat{j}_{m,n}, \tag{61}$$

where $\hat{j}_{m,n}=F(j)$. Here F(f) means the DFT of the function f. After obtaining the Fourier components $\hat{\psi}_{m,n}$ and $\hat{c}_{m,n}$ by solving the above equations, their physical components $\psi(\tau, x, z)$ and $c_1(\tau, x, z)$ are obtained by taking the inverse discrete Fourier transform (IDFT) on their Fourier components. The ordinary differential Eq. (61) is solved using the Adams-Bashforth predictor corrector method.

3. Direct Numerical Simulation

To examine the growth behavior of disturbances, Eqs. (60) and (61) should be solved with the proper initial conditions. However, we do not know what initial conditions exist at $\tau=0$. The selection of the proper initial conditions is a complex question. From the linear stability analysis, it is possible to construct the concentration at the excitation time $\tau=\tau_i$ as

$$c_1=\varepsilon\frac{1}{\sqrt{\sqrt{\pi}}}\exp\left(-\frac{z^2}{4\tau_i}\right)\mathrm{rand}(x), \tag{62}$$

where ε is the magnitude of the temperature disturbance at $\tau=\tau_i$. This initiation condition corresponds to $\mathbf{a}^{*}=[1, 0, 0, \ldots]^T$. Here τ_i and ε ought to be small values under $\varepsilon/\sqrt{\tau_i}<1$ since $|c_1/c_0|<1$. The relation of $\psi(\tau_i)\to 0$ is assumed since $w_1\to 0$ as $\tau\to 0$. This means that the magnitude of velocity fields is much smaller than that of the concentration disturbance.

Since many researchers are interested in the enhancement of dissolution driven by the instability motion, let us consider the rate of dissolution. The dimensionless total instantaneous flux of dissolution into the system, J, can be written as

$$J=J_0+J_1=-\frac{1}{(c_0+\bar{c}_1)\big|_{z=0}}, \tag{63}$$

where $\bar{c}_1$ is the horizontal mean of c_1. The diffusional flux, J_0, can be computed explicitly from the base concentration profile as

$$J_0=-\frac{1}{c_0\big|_{z=0}}=\frac{1}{2}\sqrt{\pi/\tau}. \tag{64}$$

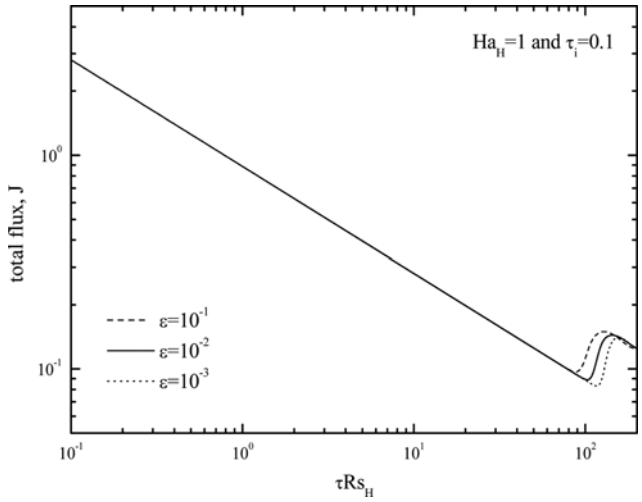

Fig. 5. The effect of the initial disturbance level on the evolution of the total flux.

We now consider the effect of the amplitude of the initial disturbance on the total flux J. In Fig. 5, we plot the total flux J for three different simulations with $Ra=10^3$ and Ha=1. Regardless of the magnitude of the initial disturbance, during the initial period, diffusion dominates over convection and the disturbances remain in the linear region. As shown in this figure, for the limiting case of $\varepsilon \to 0$, the present nonlinear analysis is reduced to the linear one and the deviation time from which the nonlinear effects are important is strongly dependent on the initiation condition. It is seen that the weaker the initial disturbance is, the longer the time at which the nonlinear terms begin to dominate is. However, for a real physical system it is difficult to characterize the amplitude and shape of initial disturbances. From now on, we use Eq. (62) with $\tau_i Rs_H=0.1$ and $\varepsilon=10^{-2}$ as the initial condition. The effect of the random number sequence on the temporal evolution of the total flux is summarized in Fig. 6. As shown, the random number sequence has little effect on the growth of the instabilities.

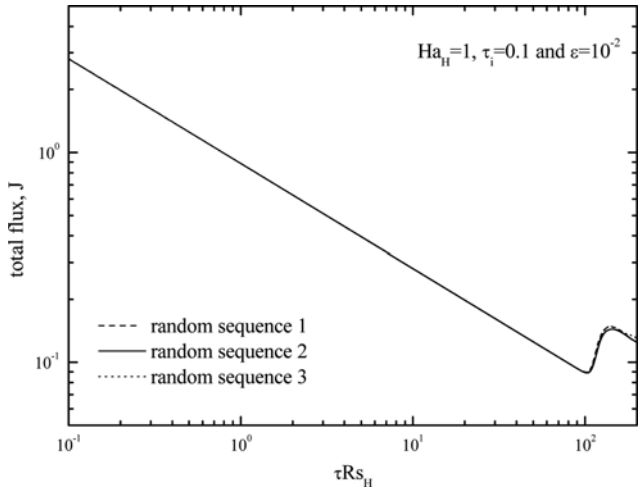

Fig. 6. The effect of the random number sequence on the evolution of the total flux.

Table 1. Comparison of critical conditions obtained from the various approximations for the limiting case of $Ha_H=0$

	n=1	n=3	n=5	n=7	Numerical shooting
$\tau_c Rs_H$	8.7296	8.6729	8.6152	8.5802	8.5392
$k_c\sqrt{\tau_c}$	0.79	0.79	0.80	0.80	0.80

RESULTS AND DISCUSSION

Noghrehabadi [24] analyzed the onset of buoyancy-driven convection of a fluid saturated in a porous medium heated from below with a constant heat flux while the upper boundary was kept at a constant temperature. Because, for the limiting case of $Ha_H=0$, their thermal system is identical with the present one for the deep-pool region, where the upper boundary condition is not important. Based on the QSSA, Noghrehabadi [24] suggested the following critical conditions:

$$\tau_c Rs_H=8.538205 \text{ and } k_c^*=0.797656 \tag{65}$$

which are nearly the same as the present ones which are summarized in Table 1. In their QSSA, they expressed $c_1(\tau, \zeta)=\Theta(\zeta)\exp(\lambda s)$, here $s=\sqrt{\tau Rs_H}$, and suggested $\lambda s=-1$ for the long-wave disturbance, i.e.. k=0. By considering the relations

$$\sigma^*=\frac{1}{|c_1|}\frac{d|c_1|}{d\tau} \text{ and } \lambda=\frac{1}{|c_1|}\frac{d|c_1|}{ds}, \tag{66}$$

we can get $\sigma^*\tau=\lambda s/2=-1/2$, which is identical with Eq. (46b). In Noghrehabadi's [24] parabolic simulations, they also solved the stability Eqs. (24)-(26) numerically under the following initial condition:

$$c_1(\tau, \zeta)=\exp(-\zeta^2/4) \text{ at } \sqrt{\tau Rs_H}=0.1. \tag{67}$$

Note that the above initial conditions are the same as the present least stable initial disturbance, which is identified in Eq. (46). Furthermore, their parabolic simulation can be mimicked by solving

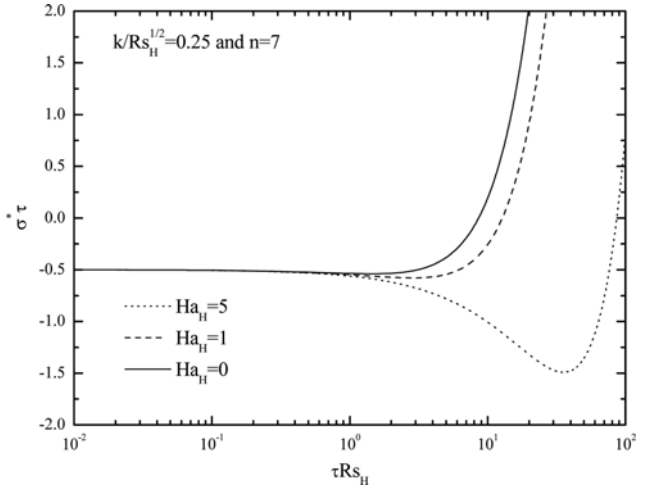

Fig. 7. Effect of Ha_H on the growth rate of the instability for the specific case of $k/Rs_H=0.25$. The growth rates are calculated using seven terms under the GSA.

the system of the simultaneous ordinary differential equations, Eq. (40), under the above initial condition. Based on the above findings, for the limiting case of Ha_H=0, the present analysis explains the previous work.

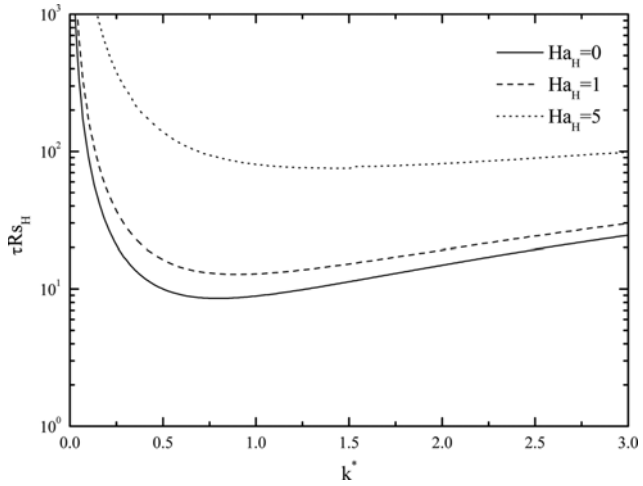

Fig. 8. Neutral stability curves obtained from the GSA for the various Ha_H values.

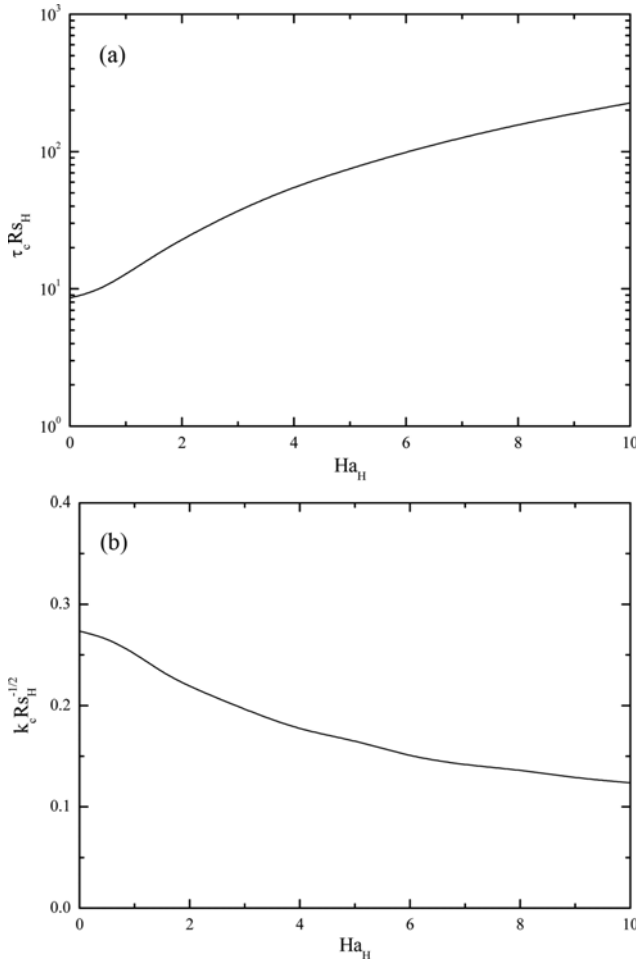

Fig. 9. Effect of Ha_H on the critical conditions. (a) Onset time, (b) critical wavenumber.

Very recently, Harfash [18] analyzed the effect of the magnetic field on the onset of buoyancy-driven convection using the energy method. He assumed the base field is fully-developed and time-independent. According to his results, the magnetic field makes the system stable. Now, let us consider the effect of magnetic field on the growth of the instabilities under the transient base field. For a specific case, the effect of the Ha_H on the growth rates calculated from the GSA is summarized in Fig. 7. This figure indicates that the magnetic field makes the system stable and retards the growth of instabilities. By employing the GST, the neutral stability curves for the various Ha_H are compared in Fig. 8. The minimum points of each curve, which are corresponding to the onset times, are summarized in Fig. 9. Figs. 7-9 imply that the magnetic field has a critical effect on the onset of convective instability, i.e., the magnetic retards the onset of instability. This means that the Lorentz force term, $Ha_H^2(\mathbf{u}\times\mathbf{e}_z)\times\mathbf{e}_z$ in Eq. (14), makes the system stable. The magnetic field effect can be easily understood by considering the relation: $Ha_H^2(\mathbf{u}\times\mathbf{e}_z)\times\mathbf{e}_z=-Ha_H^2\mathbf{e}_x(\mathbf{u}\cdot\mathbf{e}_x)$. This relation means that the magnetic field restricts a lateral motion. Thus, the Lorentz force makes the system stable through an additional resistance for the lateral motion.

For the various Ha_H, total fluxes calculated from the present DNS are summarized in Fig. 10. As shown, the present τ_c obtained from the linear stability theory is much shorter than τ_m at which the total flux shows its minimum. This means that the growth period during which the convective motion grows enough to be apparent is much larger than the τ_c. For the case of Ha_H=0.5, the temporal evolution of the concentration disturbance, c_1, is featured in Fig. 11. The instability grows as fingers and its intensity increase as time goes by. It is interesting that the convective motion is not sensible for $\tau\leq 50$ even though the critical time determined from the linear stability theory is τ_c=9.701. This means that a longer growth period is required for the instability motion to be visible. For a fixed time, the effect of the Ha_H on the development of the concentration disturbance is explained in Fig. 12. As shown, it is clear that the magnetic field restricts the growth of the instability motion.

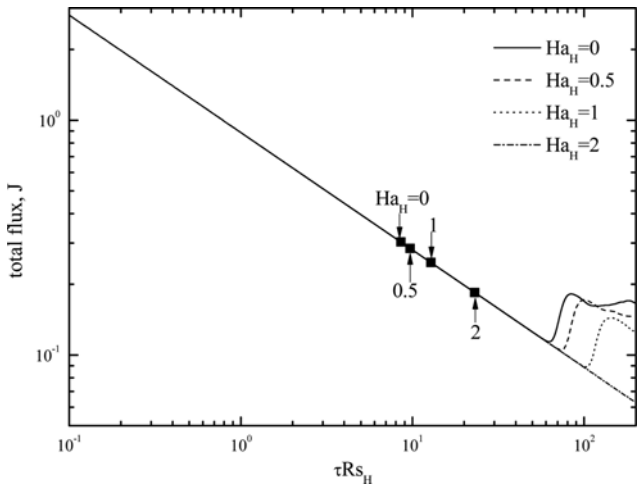

Fig. 10. Effect of Ha_H on the temporal evolution of the total flux. ■ represents τ_c from the linear stability analysis.

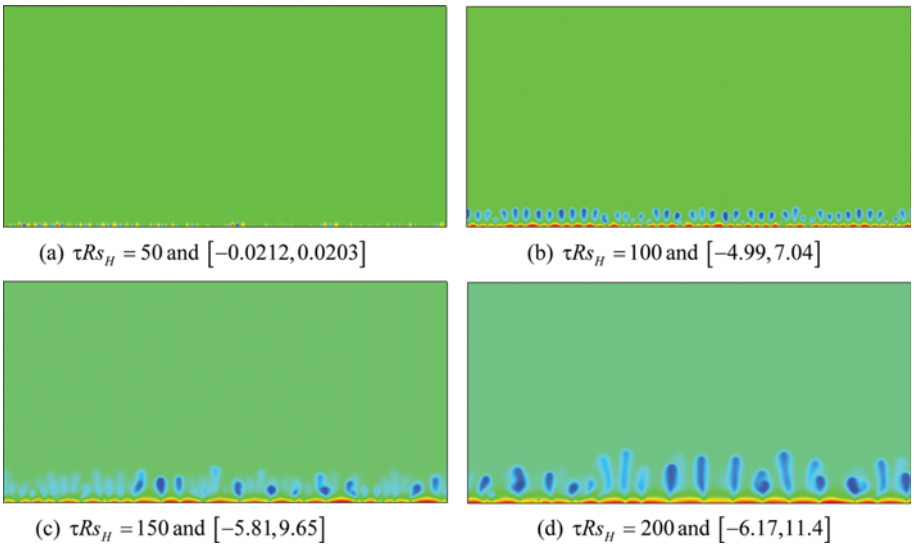

Fig. 11. Temporal evolution of concentration disturbance fields for Ha_H=0.5 and Rs_H=1000. The numbers in the parenthesis are the minimum and maximum of c_1, i.e., $[c_{1,min}, c_{1,max}]\times Rs_H$ at each τ. Plotting domain is [0, 1]×[0, 0.5].

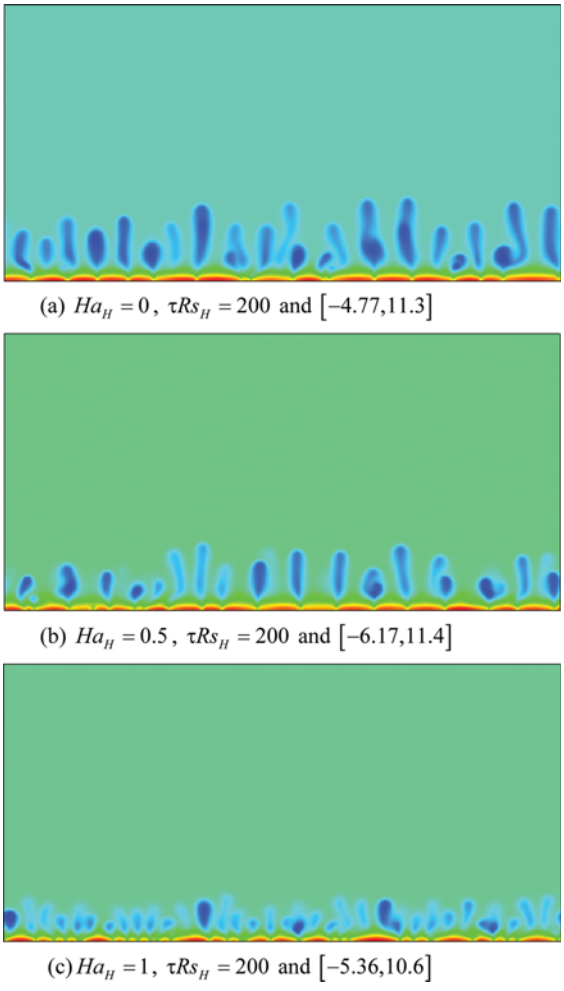

Fig. 12. The effect of Ha_H on the distribution of concentration disturbance for Rs_H=1000. The numbers in the parenthesis are the minimum and maximum of c_1, i.e., $[c_{1,min}, c_{1,max}]\times Rs_H$ at each τ. Plotting domain is [0, 1]×[0, 0.5].

For a homogeneous fluid medium, Messlinger et al. [8] conducted experiments to determine the onset time of Soret convection for the bottom heating case. Their onset times determined from particle tracking method are very close to the previous linear and nonlinear stability analysis results for a homogeneous fluid medium [9,12] and those from the shadow graph technique are very close to Messlinger et al's [8] scaling relation. Even though previous linear and nonlinear stability analyses compared quite well with the thermal convection system, systematic experiments on the magnetic field on the onset of Soret convection in a Hele-Shaw cell are required to validate the present stability results. Recently, using a Soret-driven convection in a nanofluid, Donzell et al. [31] and Bernardin et al. [32] devised a tunable bistable heat transfer device where the heat transfer rate is significantly changed even if the difference between the imposed temperatures is very small. They control the heat transfer rate by the time-programmed temperature difference. Because we can control the Soret-convection motion by a magnetic field, the present study suggests another possibility for devising a smart heat transfer device.

CONCLUSIONS

Under a uniform magnetic field, the onset of convective motion driven by Soret diffusion in an initially quiescent, vertical Hele-Shaw cell was analyzed by using the linear stability theory. By taking the Lorenz force into account, new stability equations were derived in the global domain and were transformed in the semi-infinite one. With and without the quasi-steadiness assumptions, the resulting stability equations were solved analytically by expanding the disturbances as a series of orthogonal functions and, also, the numerical shooting method was used. The linear stability limits were independent of the solution methods. Because the magnetic field plays a critical role in the onset of Soret-convection, we have another option to control the onset of convective instability in a nanoparticles-suspension system.

ACKNOWLEDGEMENT

This research was supported by the 2016 scientific promotion program funded by Jeju National University.

NOMENCLATURE

B : magnetic field vector [T]
b : thickness of Hele-Shaw cell [m]
C : concentration [wt%]
c : dimensionless concentration, $D_C(C-C_i)/(j_S d)$
D_C : diffusion coefficient [m^2/s]
D_T : Soret diffusion coefficient
d : height of Hele-Shaw cell [m]
($\mathbf{e}_x$, $\mathbf{e}_z$) : unit vector in *x*- and *z*-direction
g : gravitational acceleration vector [m/s^2]
Ha_H : Hele-Shaw Hartmann, $Ha_H=B_0(\sigma K/\mu)^{1/2}$
J : electric current vector [A]
j : mass flux [$kg/(m^2 s)$]
j_S : mass flux due to the Soret effect, $j_S=D_T\Delta T/d$
K : permeability, $b^2/12$
k : dimensionless wavenumber
k^* : modified dimensionless wave number, $k\sqrt{\tau}$
Le : Lewis number, D_C/α
P : pressure [Pa]
Ra_H : Hele-Shaw Rayleigh number, $g\beta\Delta TKd/(\alpha\nu)$
Rs_H : Hele-Shaw Rayleigh number based on the Soret flux, $Ra_H(\chi/Le)$
T : temperature [K]
t : time [s]
U : velocity vector [m/s]
w : dimensionless vertical velocity component
(x, y, z) : dimensionless Cartesian coordinates

Greek Symbols

α : thermal diffusivity [m^2/s]
β_C : concentration expansion coefficient, $\rho^{-1}(\partial\rho/\partial C)$
β_T : thermal expansion coefficient, $\rho^{-1}(\partial\rho/\partial T)$
ζ : similarity variable, $(z/\sqrt{\tau})$
η : magnetic diffusivity [m^2/s]
θ : dimensionless temperature, $(T_i-T)(T_i-T_u)$
μ : viscosity [Pa·s]
ν : kinematic viscosity [m^2/s]
ρ : density [kg/m^3]
σ : electrical conductivity [S/m]
τ : dimensionless time, $[\alpha t/d^2]$
χ : separation ratio, $\beta_C D_T/(\beta_T D_C)$

Subscripts

c : critical condition
i : initial state
0 : basic quantity
1 : perturbed quantity

REFERENCES

1. R. Taylor, S, Coulombe, T. Otanicar, P. Phelan, A. Gunawan, W. Lv, G. Rosengarten, R. Prasher and H. Tyagi, *J. Appl. Phys.*, **113**, 011301 (2013).
2. A. Ryskin and H. Pleiner, *Phys. Rev. E*, **71**, 056303 (2005).
3. R. Cerbino, A. Vailati and M. Giglio, *Phys. Rev. E*, **66**, 055301 (2002).
4. R. Cerbino, A. Vailati and M. Giglio, *Phiilos Mag.*, **83**, 2023 (2003).
5. R. Cerbino, S. Mazzoni, A. Vailati and M. Giglio, *Phys. Rev. Lett.*, **94**, 064501 (2005).
6. S. Mazzoni, R. Cerbino, D. Brogioli, A. Vailati and M. Giglio, *Eur. Phys. J. E*, **15**, 305 (2004).
7. F. Winkel, S. Messlinger, W. Schöpf, I. Rehberg, M. Siebenbürger and M. Ballauff, *New J. Phys.*, **12**, 053003 (2010).
8. S. Messlinger, C. Kramer, J. J. Schmied, F. Winkel, W. Schöpf and I. Rehberg, *Phys. Rev. E*, **88**, 053019 (2013a).
9. M. C. Kim, J. S. Hong and C. K. Choi, *AIChE J.*, **52**, 2333 (2006).
10. M. C. Kim and C. K. Choi, *Phys. Rev. E*, **76**, 036302 (2007).
11. M. C. Kim, *Eur. Phys. J. E*, **34**, 27 (2011).
12. M. C. Kim, *Korean J. Chem. Eng.*, **30**, 831 (2013).
13. S. Messlinger, W. Schöpf and I. Rehberg, *Int. J. Heat Mass Transfer*, **62**, 336 (2013).
14. L. N. Howard, Convection at high Rayleigh number, in: H. Görtler (Ed.), Proceedings of 11th International Congress of Applied Mechanics, Münich (Germany), 1109 (1964).
15. W. Schöpf, *J. Fluid Mech.*, **245**, 263 (1992).
16. M. C. Kim, *Int. J. Non-Linear Mech.*, **67**, 291 (2014).
17. S. Chandrasekhar, *Hydrodynamic and Hydromagnetic Stability*, Oxford Univ. Press (1961).
18. A. J. Harfash, *Transp Porous Med.*, **103**, 361 (2014).
19. H. Heidary, R. Hosseini, M. Pirmohammadi and M. J. Kermani, *J. Magn. Magn. Mater.*, **374**, 11 (2015).
20. G. P. Galdi and B. Straughan, *Arch. Rational Mech. Anal.*, **89**, 211 (1985).
21. A. Riaz, M. Hesse, H. A. Tchelepi and F. M. Orr Jr., *J. Fluid Mech.*, **548**, 87 (2006).
22. A. Selim and D. A. S. Rees, *J. Porous Media*, **10**, 1 (2007).
23. M. C. Kim and C. K. Choi, *Korean J. Chem. Eng.*, **32**, 2400 (2015).
24. A. Noghrehabadi, D. A. S. Rees and A. P. Bassom, *Transp. Porous Med.*, **99**, 493 (2013).
25. M. C. Kim and C. K. Choi, *Chem. Eng. Sci.*, **98**, 255 (2013).
26. W. M. Deen, *Analysis of Transport Phenomena*, Oxford Univ. Press (1997).
27. B. F. Farrell and P. J. Ioannou, *J. Atmos. Sci.*, **53**, 2041 (1996).
28. M. C. Kim and C. K. Choi, *Phys. Fluids*, **24**, 044102 (2012).
29. M. C. Kim, *Korean J. Chem. Eng.*, **30**, 1207 (2013).
30. C. T. Tan and G. M. Homsy, *Phys. Fluids*, **31**, 1330 (1988).
31. G. Donzelli, R. Cerbino and A. Vailati, *Phys. Rev. Lett.*, **102**, 104503 (2009).
32. M. Bernardin, F. Comitani and A. Vailati, *Phys. Rev. E*, **85**, 066321 (2012).